Human Molecular Genetics, 2015, Vol. 24, No. 22 6278–6292

doi: 10.1093/hmg/ddv334
Advance Access Publication Date: 24 August 2015
Original Article

ORIGINAL ARTICLE

Muscle weakness in *TPM3*-myopathy is due to reduced Ca^{2+}-sensitivity and impaired acto-myosin cross-bridge cycling in slow fibres

Michaela Yuen[1,2,*], Sandra T. Cooper[1,2], Steve B. Marston[3], Kristen J. Nowak[4], Elyshia McNamara[4], Nancy Mokbel[1,5], Biljana Ilkovski[1], Gianina Ravenscroft[4], John Rendu[6], Josine M. de Winter[7], Lars Klinge[8], Alan H. Beggs[9], Kathryn N. North[1,2,10,11], Coen A.C. Ottenheijm[7,†] and Nigel F. Clarke[1,2,†]

[1]Institute for Neuroscience and Muscle Research, The Children's Hospital at Westmead, Westmead, Australia, [2]Discipline of Paediatrics and Child Health, University of Sydney, Sydney, Australia, [3]National Heart and Lung Institute, Imperial College London, London, UK, [4]Harry Perkins Institute of Medical Research and the Centre for Medical Research, University of Western Australia, Nedlands, Australia, [5]Faculty of Health Sciences, St. George Health Complex, The University of Balamand, Beirut, Lebanon, [6]Département de Biochimie Toxicologie et Pharmacologie, Département de Biochimie Génétique et Moléculaire, Centre Hospitalier Universitaire de Grenoble, Grenoble, France, [7]Department of Physiology, Institute for Cardiovascular Research, VU University Medical Center, Amsterdam, The Netherlands, [8]Department of Pediatrics and Adolescent Medicine, Division of Pediatric Neurology, Faculty of Medicine, Georg August University, Göttingen, Germany, [9]Division of Genetics and Genomics, The Manton Center for Orphan Disease Research, Boston Children's Hospital, Harvard Medical School, Boston, MA, USA, [10]Murdoch Children's Research Institute, the Royal Children's Hospital, Parkville, Australia and [11]Department of Paediatrics, University of Melbourne, Melbourne, Australia

*To whom correspondence should be addressed at: Institute for Neuroscience and Muscle Research, The Children's Hospital at Westmead, Locked Bag 4001, Westmead, NSW 2145, Australia. Tel: +61 298451495; Fax: +61 298453489; Email: michaela.kreissl@sydney.edu.au

Abstract

Dominant mutations in *TPM3*, encoding α-tropomyosin$_{slow}$, cause a congenital myopathy characterized by generalized muscle weakness. Here, we used a multidisciplinary approach to investigate the mechanism of muscle dysfunction in 12 *TPM3*-myopathy patients. We confirm that slow myofibre hypotrophy is a diagnostic hallmark of *TPM3*-myopathy, and is commonly accompanied by skewing of fibre-type ratios (either slow or fast fibre predominance). Patient muscle contained normal ratios of the three tropomyosin isoforms and normal fibre-type expression of myosins and troponins. Using 2D-PAGE, we demonstrate that mutant α-tropomyosin$_{slow}$ was expressed, suggesting muscle dysfunction is due to a dominant-negative effect of mutant protein on muscle contraction. Molecular modelling suggested mutant α-tropomyosin$_{slow}$ likely impacts actin–tropomyosin interactions and, indeed, co-sedimentation assays showed reduced binding of mutant α-tropomyosin$_{slow}$ (R168C) to filamentous actin. Single fibre contractility studies of patient myofibres revealed marked slow myofibre specific abnormalities. At saturating [Ca^{2+}] (pCa 4.5), patient slow fibres produced only 63% of the contractile force produced in control slow fibres and

†The authors wish it to be known that, in their opinion, the last two authors should be regarded as joint last authors.

Received: May 28, 2015. **Revised:** July 20, 2015. **Accepted:** August 10, 2015

had reduced acto-myosin cross-bridge cycling kinetics. Importantly, due to reduced Ca^{2+}-sensitivity, at sub-saturating [Ca^{2+}] (pCa 6, levels typically released during *in vivo* contraction) patient slow fibres produced only 26% of the force generated by control slow fibres. Thus, weakness in *TPM3*-myopathy patients can be directly attributed to reduced slow fibre force at physiological [Ca^{2+}], and impaired acto-myosin cross-bridge cycling kinetics. Fast myofibres are spared; however, they appear to be unable to compensate for slow fibre dysfunction. Abnormal Ca^{2+}-sensitivity in *TPM3*-myopathy patients suggests Ca^{2+}-sensitizing drugs may represent a useful treatment for this condition.

Introduction

Dominant mutations in the *TPM3* gene, encoding α-tropomyosin$_{slow}$ (α-TPM$_{slow}$), cause a congenital myopathy characterized by mild to moderate early onset, non-progressive generalized muscle weakness (1–3). Axial and respiratory muscles are commonly involved and many patients require night-time ventilatory support (1,2). Recessive mutations, causing loss of protein, are rare with only four instances reported to date in patients with relatively severe clinical presentations (2,4–6). In contrast, more than 40 families with dominant *TPM3* missense mutations have been identified involving 19 different residues (1–3,7–12) (Supplementary Material, Table S1). Histologically, many *TPM3* patients present with slow skeletal myofibre hypotrophy in the absence of additional pathological features, resulting in a clinical diagnosis of congenital fibre-type disproportion (CFTD) (3). Some patients also exhibit nemaline bodies or cores in myofibres and are classified as nemaline myopathy (7) or core myopathy (1,10,13), respectively. The same mutation in *TPM3* can cause a variety of histological phenotypes (Supplementary Material, Table S1) (1–3,13).

Three tropomyosin isoforms are present in the skeletal muscle sarcomere (14). *TPM1* and *TPM3* encode the two α-tropomyosins expressed exclusively in fast fibres [*TPM1*; α-tropomyosin$_{fast}$ (α-TPM$_{fast}$), Tpm1.st] or slow fibres (*TPM3*; α-TPM$_{slow}$, Tpm3.12st), respectively. *TPM2* encodes β-tropomyosin (β-TPM, Tpm2.2st) and is expressed in both fibre types (14–16). Tropomyosin forms alpha-helical coiled-coil heterodimers between one α- and one β-chain. These dimers polymerize head-to-tail into a continuous filament that associates along the entire length of the actin thin filament and interacts with the troponin complex to regulate Ca^{2+}-mediated actin-myosin cross-bridge cycling during muscle contraction. The structure of tropomyosin is conferred by a seven residue repeat motive [*a-b-c-d-e-f-g*] (Fig. 1A and B) (17). Residues at positions *a* and *d* in the repeat are typically hydrophobic, creating a hydrophobic pocket between two tropomyosin chains facilitating dimerization (blue). Charged residues at positions *g* and *e* (green) stabilize the dimer through inter-helical salt bridges. Positions *b*, *c* and *f* (yellow) localize to the surface of tropomyosin dimers and likely modulate interactions with proteins such as actin and troponin.

Many dominant *TPM3* mutations (11/19) affect positions *b*, *c* or *f* on the outer surface of the dimer (Fig. 1C, yellow). Only five mutations affect positions *a* and *d* in the hydrophobic pocket (Fig. 1C, blue) and three mutations affect positions *g* and *e* constituting the inter-helical salt bridges (Fig. 1C, green). All mutations fall within, or very close to, one of the seven actin-binding regions of tropomyosin (Fig. 1C, purple shaded area of the molecule) (20). In particular, there is a striking concentration of mutations within the fifth actin-binding region of α-TPM$_{slow}$ (R168H, R168G, R168C, K169E, E174A) some of which are recurrent in several unrelated families (e.g. R168 residue is mutated in 20 different families).

Although the structure and function of tropomyosin is well established, the mechanism(s) by which mutations in *TPM3* cause muscle weakness remains poorly understood. Two recent studies showed that four patients with dominant *TPM3* mutations had abnormal cross-bridge cycling kinetics and Ca^{2+}-sensitivity of contraction in single skeletal myofibres isolated from patient biopsies [$n = 3$ (21), $n = 1$ (22)]. However, these studies were limited by small sample sizes, and separate assessment of the properties of slow versus fast myofibres was only possible to a limited extend. In this study, we aimed to unravel the mechanism of muscle weakness in a cohort of 12 patients with dominant *TPM3* mutations. We performed thorough histological characterization, assessed thin filament protein expression and quantified the contractile properties of single myofibres isolated from patient muscle specimens (10/12 patients, Table 1).

Results

TPM3-myopathy patients have slow fibre hypotrophy and deregulation of slow and fast muscle fibre proportions

The main histological characteristic in all patients with *TPM3* mutations is selective hypotrophy of slow-twitch type-1 fibres, compared with fast-twitch type-2 fibres (1–3) (Fig. 2A, ATPase pH 4.6, slow myofibres appear dark; see Supplementary Material, Table S2 for measurements). On average, fast fibres were between 1.7 and 5.2 times larger in diameter than slow fibres (Fig. 2B), corresponding to a percentage fibre-size disproportion (%FSD) of 41–78.3% (Fig. 2C). The selective hypotrophy of slow fibres in *TPM3* patients is consistent with the slow-fibre specific expression of α-TPM$_{slow}$.

Additionally, fibre-typing was skewed in patient biopsies, either towards fast fibre predominance (five patients, less than 30% slow fibre area) or slow fibre predominance (six patients, more than 60% slow fibre area), compared with age-matched control biopsies where the cross sectional area (CSA) occupied by either fibre-type is approximately 50:50 [this study and (18,23)] (Fig. 2D). Only one patient biopsy showed normal slow-fast fibre distribution (between 40 and 60% slow fibre area).

Tropomyosin isoform ratios are not commonly altered in TPM3-myopathy patients

In normal muscle, the ratio of α/β tropomyosin molecules is approximately 50:50 β-TPM/α-TPM$_{fast}$ in fast fibres and 50:50 β-TPM/α-TPM$_{slow}$ in slow fibres (24). A patient and transgenic mouse model carrying the *TPM3* M9R mutation, the first mutation associated with nemaline myopathy, showed an imbalance of this ratio, with a dramatic excess of α-TPM$_{slow}$ relative to β-TPM in skeletal muscle (25) (Fig. 3Ai, Lane 5). This disruption in tropomyosin stoichiometry was proposed as a potential mechanism of muscle weakness (25). In contrast, in this cohort of 12 *TPM3*-myopathy patients, we observed normal ratios of α/β tropomyosin, similar to controls (Fig. 3Ai). The scatter plots in Figure 3Aii–iiii show the relative levels of each tropomyosin isoform relative to the type-1 fibre CSA, as determined by ATPase staining. β-TPM is present at equal amounts in slow and fast myofibres in all

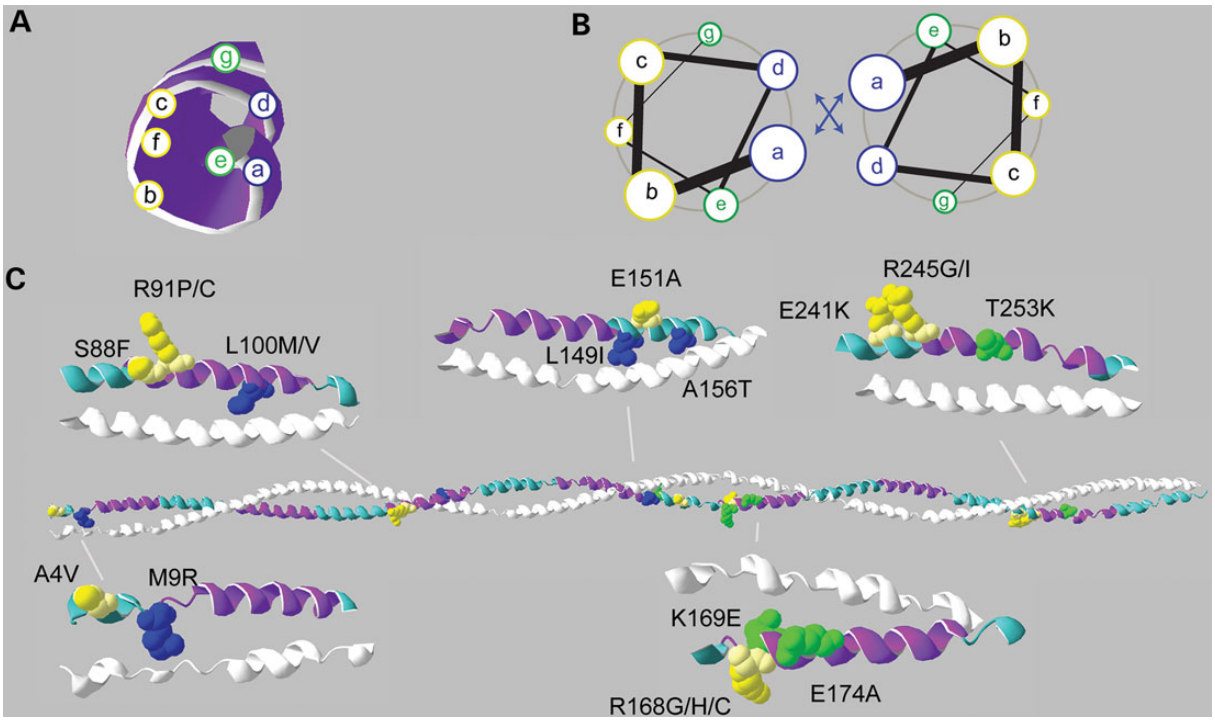

Figure 1. Dominant mutations in *TPM3* affect amino acids located within or close to actin-binding domains. Tropomyosins form α-helical coiled-coil dimers via a seven residue repeat motive in their amino acid sequence [*a-b-c-d-e-f-g*] as illustrated in (**A**) and (**B**). Positions *a* and *d* (blue) are usually hydrophobic and create a hydrophobic pocket between two tropomyosin chains facilitating dimerization in a 'knobs-into-holes' fashion. Positions *g* and *e* (green) are occupied by charged amino acids that further stabilize the dimer through inter-helical salt bridges. Positions *b*, *c* and *f* (yellow) localize to the surface of the TM dimer and likely modulate interactions with protein binding partners such as actin and troponin. (**C**) A ribbon model of a whole tropomyosin dimer with the actin-binding domains marked in pink on one strand. The residues affected by dominant mutations in *TPM3* are shown. All affected residues are located in or close to actin-binding domains. Eight mutations affect residues in the *b*, *c* or *f* positions of the repeat (yellow). Three mutations affect residues in the *a* and *d* position (blue) and two affect residues in the *g* and *e* position (green). RCSB Protein Data Bank access code for protein structure model is 1C1G [tropomyosin dimer, Whitby and Phillips (18)]. Swiss-PDB Viewer v4.1.0 was used to create molecular graphics (19).

Table 1. Patient cohort with dominant TPM3 mutations

P	Mutation in *TPM3*	Disease	Muscle type	Sex	Age at biopsy	Clinical classification	Publication	Contractile studies
1	K169E	CFTD	Q	M	16 months	Moderate	(1): P 2	Y
2	R245G	CFTD	Q	M	20 months	Moderate	(1): P 1	Y
3a	L100M	CFTD	Q	F	3 years	Mild	(1): P 5	Y
3b	L100M	CFTD	B	M	30 years	Mild	(1): P 7	Y
3c	L100M	CFTD	B	M	36 years	Mild	(1): P 8	Y
4	R168G	CFTD	Q	M	10 years	Mild	(1): P 3	Y
5	R168H	CFTD	Q	F	40 years	Mild	Unpublished	Y
6a	R168H	NM	D	F	20 years	Mild	(1): P 10	N
6b	R168H	CFTD	?	M	56 years	Mild	(1): P 11	Y
7	R168C	Cap	?	M	3 years	Mild	(13): P 1	Y
8	R168C	CFTD	Q	F	19 years	Moderate	(1): P 9	Y
9	M9R	NM	Q	F	21 years	Mild	(7); (37): P 1	N
10	R168H	NM	D	M	53 years	Mild	(12): P III-4	N
11	E241K	CFTD	Q	F	0.5 year	Moderate	(2): P 311-1	N
12	R91P	CFTD	Q	F	0.5 year	Severe	(2): P 913-1	N

Q, quadriceps; B, biceps; D, deltoid; P, patient.
The numbers in parentheses of column 'Publication' refer to the references these patients were published in. Additionally, this column gives information on the patient identifier used in the study (eg. P2 = patient 2).

samples (~50% of total tropomyosin, Fig. 3Aii). The relative expression of α-TPM_{slow} and α-TPM_{fast} correlates well with type-1 fibre CSA (positive correlation for α-TPM_{slow} and negative correlation for α-TPM_{fast}, Fig. 3Aiii and Aiiii). The linear regression slope fitted to the data was not significantly different between patients and controls, demonstrating a normal ratio of α/β tropomyosin isoforms in fast and slow fibres.

Mutant α-TPM_{slow} is expressed in muscle of TPM3-myopathy patients

The autosomal dominant inheritance of *TPM3* mutations within our cohort is consistent with the hypothesis that mutant α-TPM_{slow} is expressed in slow skeletal myofibres and causes disease via a dominant-negative effect on thin filament function.

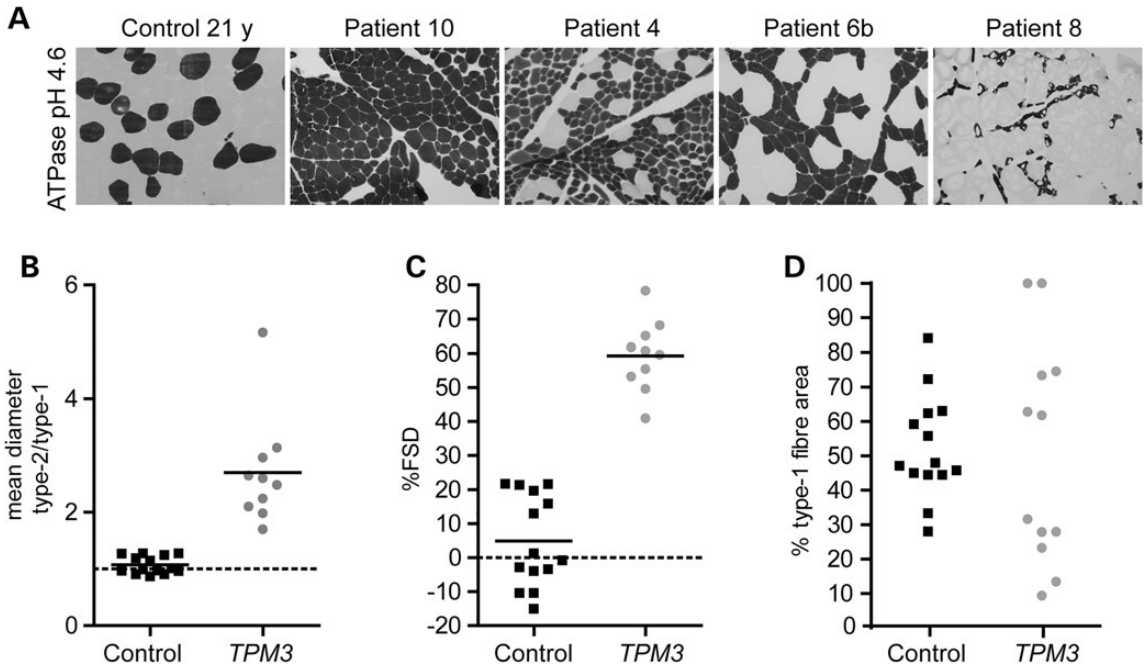

Figure 2. *TPM3*-myopathy patients have slow fibre hypotrophy and a deregulation of slow and fast muscle fibre proportions. (**A**) ATPase pH 4.6 stained muscle cross section of one control and four patients with mutations at residue R168, of α-TPM_{slow} demonstrating a selective hypotrophy of slow type-1 myofibres. Fast type-2 fibres are between 1.7 and 5.2 times larger in size than type-1 fibres, whereas age-matched controls (age between 0.8 and 57 years) showed roughly equally sized fibres (**B**). This corresponds to a fibre-size disproportion (FSD) between 41 and 78.3% (**C**). Patients with *TPM3* mutations show an abnormal fibre type distribution ranging from complete type-1 fibre predominance (A: Patient 10) to type-2 fibre predominance (A: Patient 8). (**D**) In the majority of control biopsies between 40 and 60% of the CSA is composed of type-1 fibres. *TPM3*-myopathy patients have either below 40% or above 60% type-1 fibre area. Fibre type measurements were performed twice at different times from the same biopsy in Patients 2, 3c, 6b and 8 (also see Supplementary Material, Table S2) and the plotted values represent the average of both measurements. All images were taken at 100× magnification. Fibre size measurements and further information on patient and control biopsies are summarized in Supplementary Material, Table S2.

To confirm mutant α-TPM_{slow} is present in patient muscle, we isolated the filamentous fractions (representing proteins incorporated in high-molecular weight structures such as sarcomeres) and performed two-dimensional SDS polyacrylamide gel electrophoresis (2D-SDS-PAGE). Five patients in our cohort from whom skeletal muscle samples were available, had a mutation that resulted in an amino-acid substitutions affecting a charged residue leading to a predicted alteration in the isoelectric point (pI) of α-TPM_{slow}. Thus, isoelectric focusing allowed us to separate the mutant from the wild-type protein on the basis of charge in these patients, and the second dimension urea-SDS gel separated the three tropomyosin isoforms from each other. The mutant α-TPM_{slow} protein could then be observed as a left-sided (Fig. 3B; R186G, R91P, K169E, R168C) or right-sided shift (Fig. 3B, E241K) from the wild-type α-TPM_{slow} and was present in all patient muscles. The total pool of α-TPM_{slow} (both wild-type and mutant isoforms) correlated with the slow fibre CSA (% type-1 fibre area annotated above each blot, see Supplementary Material, Table S2 for measurements). However, mutant α-TPM_{slow} was less abundant compared with wild-type, ranging from 27 to 45% of total α-TPM_{slow} (% mutant α-TPM_{slow} annotated on each blot).

The actin-binding properties of K169E and R168C mutant α-TPM_{slow} proteins are altered

The position of many *TPM3* mutations within or close to actin-binding sites suggests most mutations may influence interactions between α-TPM_{slow} and actin filaments. Therefore, we performed actin-tropomyosin co-sedimentation assays with two recombinant mutant α-TPM_{slow} proteins (R168C and K169E) and compared their actin-binding properties to wild-type α-TPM_{slow}. These mutations were chosen because they are both located in the fifth actin-binding domain, the area that harbours a hotspot for myopathy causing mutations, and affect amino acids predicted to be involved in actin interactions. We co-sedimented incremental amounts of each of the three α-TPM_{slow} proteins with 100 nM filamentous skeletal actin. Figure 4A shows a representative SDS-PAGE of the filamentous fraction isolated following ultracentrifugation, demonstrating dose-dependent binding of wild-type α-TPM_{slow} to actin filaments. Densitometry data of the bound fraction versus the total amount of α-TPM_{slow} added to the reaction were fitted to a Hill equation, to determine the binding constant K_d and the Hill coefficient (h) for all three α-TPM_{slow} proteins (Fig. 4B). The α-TPM_{slow} R168C protein showed reduced actin-binding affinity compared with wild-type or the α-TPM_{slow} K169E protein (K_d = 771.4 ± 188.6 nM for R168C, 180.2 ± 37.6 nM for wild-type and 164.0 ± 110.6 nM for K169E, range represents 95% confidence interval). The Hill coefficient was similar in all three mutations (h = wild-type 4.471 ± 3.0, R168C 3.308 ± 2.4, K169E 1.602 ± 1.3). These results suggest actin binding may be the mechanism by which the *TPM3* R168C mutation alters contractile function and causes muscle weakness.

Fast fibre specific α-actinin-3 is ectopically expressed in slow fibres of patients with R168H/G TPM3 mutations

As many *TPM3* patient biopsies displayed a skewing to either slow- or fast-fibre predominance by ATPase stain, we stained serial muscle sections with antibodies recognizing fibre-type-specific isoforms of myosin heavy chain (MHC), troponin and

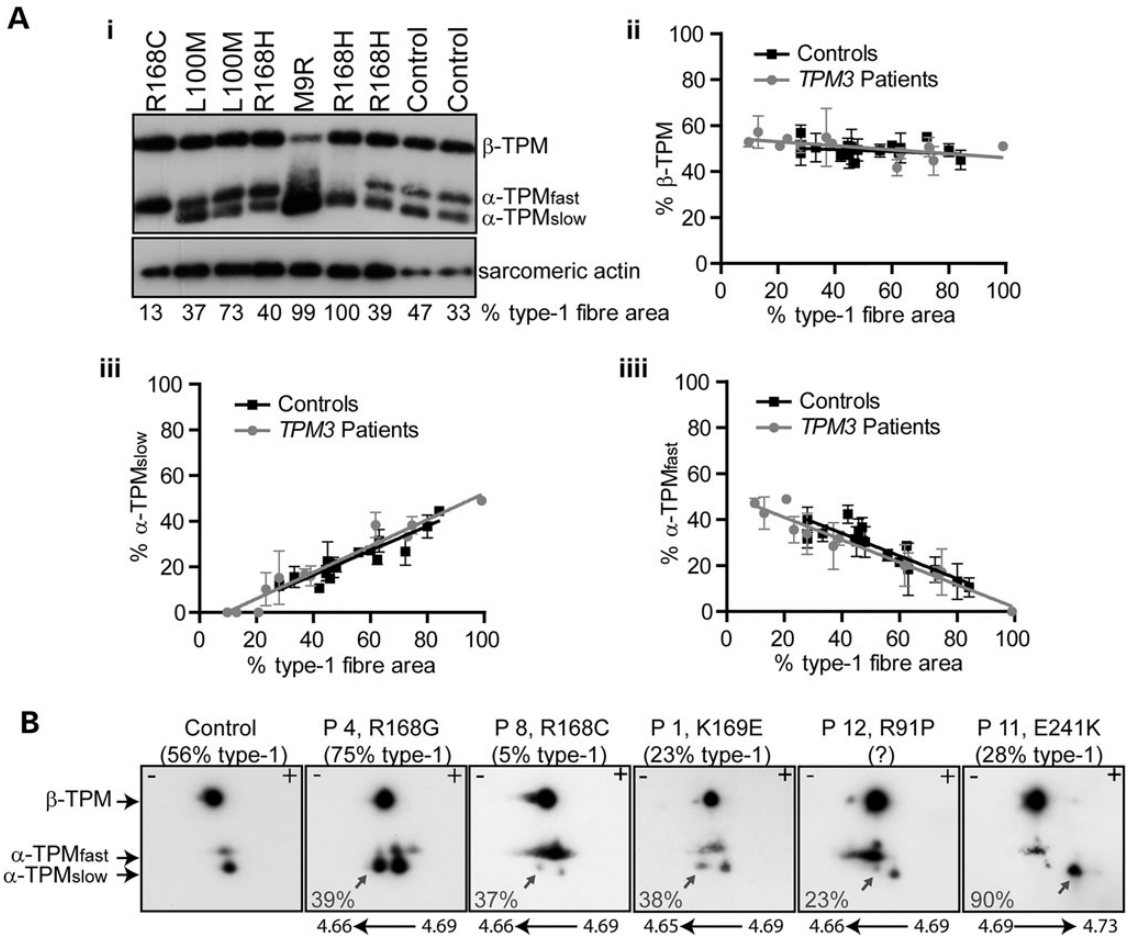

Figure 3. Tropomyosin isoform ratios are not commonly altered and mutant α-TPM_{slow} is expressed in *TPM3*-myopathy patient muscle. (**Ai**) A representative western blot of *TPM3*-myopathy patient and control muscle tissue showing the three skeletal muscle tropomyosin isoforms (β-TPM, α-TM_{fast} and α-TPM_{slow}). In normal muscle, type-1 fibres contain about 50:50 α-TPM_{slow}/β-TPM and type-2 fibres contain about 50:50 α-TPM_{fast}/β-TPM. Most sample had β-TPM and α-$TPM_{fast/slow}$ levels consistent with the relative proportion of type-1 and type-2 fibres present in the sample (% type-1 fibre area was determined from ATPase staining, see Supplementary Material, Table S2). Only one patient (*TPM3* M9R mutation, lane 5) had reduced β-TPM levels and increased expression of α-TPM_{slow} relative to other tropomyosin isoforms and the fibre type proportion in the biopsy as described previously (25). (**Aii–iiii**) Densitometry analysis of western blots from 10 patients with mutations L100M ($n = 3$), R168C ($n = 1$), R168G ($n = 1$), R168H ($n = 3$), K169E ($n = 1$), R245G ($n = 1$) was performed to quantify the proportion of each tropomyosin isoform as a percentage of total TPM. The relative abundance of each isoform was plotted against the % type-1 fibre area (measurements from *TPM3* M9R patient are not included). (Aii) β-TPM levels are about 50% of total tropomyosin in patients and controls. (Aiii–iiii) About 50% of tropomyosin is α-$TPM_{fast/slow}$, but the amount of these fibre-type-specific isoforms correlates closely with the % type-1 fibre area in both patients and controls (positive correlation for α-TPM_{slow}, negative correlation for α-TPM_{fast}). Linear regression analysis showed that slopes of patient and controls were not significantly different for any of the three isoforms ($P = 0.4997$, 0.9538 and 0.4595 for α-TPM_{slow}, α-TPM_{fast} and β-TPM, respectively). (**B**) Isoelectric focusing of patient and control muscle lysates shows three spots (corresponding to β-TPM, α-TPM_{fast}, α-TPM_{slow}). An additional spot (marked by an arrow) consistent with the predicted isoelectric point (pI) of each mutation (as annotated, wild-type α-TPM_{slow} is 4.69) is present in patient biopsies. Mutant α-TPM_{slow} accounted for 27–45% of total α-TPM_{slow} in different patient biopsies (annotated in the blot, the proportion of each tropomyosin in patient slow fibres is given in Supplementary Material, Table S3). Note the ratio of expression of α-$TPM_{fast/slow}$ depends on the percentage of slow and fast myofibres in the biopsy [e.g. Patient 8 (R168C) mainly contains fast myofibres]. Picture 3 from the left in (B) is reprinted from(13), with permission from Elsevier.

α-actinin to investigate whether the expression of several fibre-type-specific proteins was normal (Fig. 5A, Supplementary Material, Fig. S1). Three patients (Patients 4, 6a and 6b, each with R168 substitutions) showed elevated levels of hybrid fibres expressing both slow and fast myosin isoforms. All other patients showed normal fibre profiling of myosin and troponin. Curiously, when further characterizing the expression profile of hybrid fibres in Patients 4, 6a, 6b and 10, we observed ectopic expression of α-actinin-3 in dedicated slow fibres as determined by the expression of myosin and troponin (Fig. 5A, Supplementary Material, Fig. S1). α-Actinin-3 is a component of the Z-disc normally present in fast myofibres and has been found to be important for muscle performance (strength and speed) (26,27). Our results suggest that the restricted fibre-type expression profiles of α-actinin-2 and -3 is differently regulated to myosin, troponin and tropomyosin in patients with *TPM3* mutations compared with age-matched controls.

Phosphorylation of tropomyosin is increased in patients with mutations in TPM3

In normal skeletal muscle, a proportion of both α- and β-TPM is phosphorylated at residue S283 (28,29) (Fig. 5Bi). The effect of tropomyosin phosphorylation in skeletal muscle is poorly understood, but studies suggest it is important for tropomyosin function by enhancing head-to-tail interactions and increasing the cooperative activation of myosin resulting in enhanced force production (30). We investigated whether phosphorylation at S283 was altered in *TPM3* patients (as a possible contributor to muscle dysfunction) by western blot analysis using an anti-phosphor-

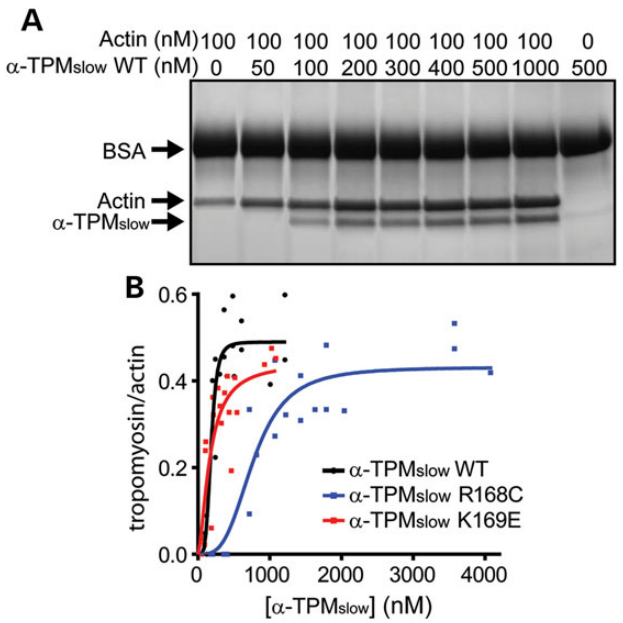

Figure 4. Mutant α-TPM_{slow} R168C proteins have a reduced affinity to filamentous actin. Phalloidin stabilized actin filaments were co-sedimented with incremental amounts of tropomyosin and the pelleted fractions were analysed by SDS-PAGE. (**A**) A representative SDS-PAGE of wild-type α-TPM_{slow} protein as was used for densitometry analysis. (**B**) The ratio of TPM/actin was plotted versus. total [TPM] added and a Hill's equation was fitted. The K_d was increased in α-TPM_{slow} R168C compared with α-TPM_{slow} wild-type and K169E suggesting weaker binding affinity to actin (771.4 ± 188.6 nM, 180.2 ± 37.6 nM, 164.0 ± 110.6 nM for α-TPM_{slow} R168C, wild-type and K169E, respectively). The Hill's coefficient *h* and maximal binding (Bmax) was similar in all three proteins (*h* = wild-type 4.471 ± 3.0, R168C 3.308 ± 2.4, K169E 1.602 ± 1.3; Bmax wild-type 0.489 ± 0.055, R168C 0.431 ± 0.078 and K169E 0.443 ± 0.156). Values are best-fit values ± 95% confidence interval.

S283 specific antibody (Fig. 5Bii shows a representative western blot). Phosphorylation of tropomyosin (all three isoforms were analysed in combination) was increased in 6/8 of patients with samples available for analysis, compared with five age-matched controls (Fig. 5Biii). However, elevated levels of S283 phosphorylation were also observed in patients with mutations in *TPM2*, *ACTA1*, *DNM2*, *DMD* and *DYSF* (Fig. 5Biiii).

Mutations in *DMD* (causing Duchenne and Becker muscular dystrophy) and *DYSF* (causing limb girdle muscular dystrophy type-2B) cause muscle fibre breakdown and regeneration. It is well documented that tropomyosin phosphorylation is higher during development in animals (29), and thus we explored whether increased phosphor-S283 in dystrophic muscle was related to fibre re-generation. Using immunohistochemistry (IHC) analysis, we established that phospho-S283 tropomyosin levels did not correlate with fibre-type or with fibre re-generation in control or patient biopsies (Supplementary Material, Fig. S2B and C). In *TPM3* patients however, levels of phospho-S283 tropomyosin were specifically elevated in small, slow-twitch myofibres (Supplementary Material, Fig. S2A). This suggests that increased phosphorylation of tropomyosin is not specific to *TPM3* disease, but may be a compensatory response to muscle dysfunction due to a variety of mechanisms.

Slow myofibres of TPM3-myopathy patients have reduced maximal force, likely due to altered cross-bridge cycling

In order to understand how muscle weakness develops in *TPM3* patients we performed contractile studies on single, chemically-permeabilised patient myofibres or small fibre bundles by immersing them in Ca^{2+}-containing solutions (see methods regarding details for analysis of bundles). This induces activation of the contractile filaments allowing measurement of isometric force production.

First, fibres and fibre bundles were activated at saturating [Ca^{2+}] of pCa 4.5 (~31.6 μM) to induce maximal isometric contraction (Fmax, Fig. 6A). A small but significant force deficit was observed in slow myofibres and fibre bundles from seven of 10 *TPM3*-myopathy patients compared with pooled control samples (Fmax in all *TPM3* patients ranges from 52.17–116 mN/mm^2 compared to 143.1 ± 31.8 mN/mm^2 in controls, $^*P < 0.01$ one-way ANOVA, Fig. 6C and D). This force deficit was present despite normalization to the smaller CSA in slow fibres of *TPM3* patients. Fmax in type-2 fibres was not different from control fibres (106.7–186.7 mN/mm^2 in patient fibres and 147.7 ± 29.34 mN/mm^2 in control fibres) (Fig. 6B). In bundles, Fmax was lower in bundles with higher slow MHC content in two of three patients (Supplementary Material, Fig. S3).

During muscle contraction, a cyclic interaction between the myosin heads and thin filaments, followed by a conformational change in myosin, allows the filaments to slide past each other. Correct positioning of tropomyosin on actin filaments during the various stages of myosin–actin interactions is crucial for efficient cross-bridge cycling. To determine if the force deficit in slow myofibres of *TPM3* patients can be attributed to changes in cross-bridge cycling kinetics we measured the rate of tension re-development (K_{tr}) during maximal activation, after a short period of unloaded shortening following by re-stretch (a typical length and force trace are presented in Fig. 7Ai). The speed of cross-bridge cycling is physiologically faster in type-2 (fast-twitch) fibres compared with type-1 (slow-twitch) fibres (see controls in Fig. 7Aii–iii). Slow fibres from eight of 10 *TPM3* patient biopsies displayed a significant reduction in K_{tr} compared with controls (K_{tr} in all *TPM3* patients ranges from 0.758–1.217 s^{-1} compared to 1.493 ± 0.25 s^{-1} in controls, $^{***}P < 0.0001$, $^*P < 0.01$, one-way ANOVA, Fig. 7Aii), whereas fast myofibres were not different from control myofibres (Fig. 7Aiii). These results suggest that myosin cross-bridge cycling kinetics are altered in slow fibres of *TPM3* patients, contributing to muscle weakness by reducing the fraction of strongly bound cross-bridges during activation.

Fmax is proportional to the force generated by a single strongly bound actin-myosin cross-bridge and the fraction of myosin heads attached to actin. We assessed active stiffness in *TPM3* biopsies, a measure proportional to the number of myosin heads strongly attached to actin during an isometric contraction (31), to study whether this contributes to muscle weakness. We measured active stiffness by performing fast length changes in isometrically contracted single myofibres (typical length/force traces are presented in Supplementary Material, Fig. S4 and a typical patient and control plot of the length change (Δ*L*) versus force change (Δ*F*) is presented in Fig. 7Bi and ii, respectively) (32). We observed a trend towards reduced absolute active stiffness in type-1 fibres and bundles/hybrid fibres of most *TPM3* patients (Fig. 7Biii and iiii), which was not present in type-2 fibres (Fig. 7Bv). The change in active stiffness was proportional to Fmax, as the difference was not present when stiffness was normalized to Fmax (Fig. 7Bvi–viii). Since stiffness is proportional to the number of strongly attached myosin cross-bridges, a reduction of active stiffness proportional to force reduction suggests that forces per cross-bridge were normal, but, in line with the reduced Ktr, the number of strongly attached cross-bridges may be reduced in slow fibres of *TPM3* patients, likely contributing to muscle weakness.

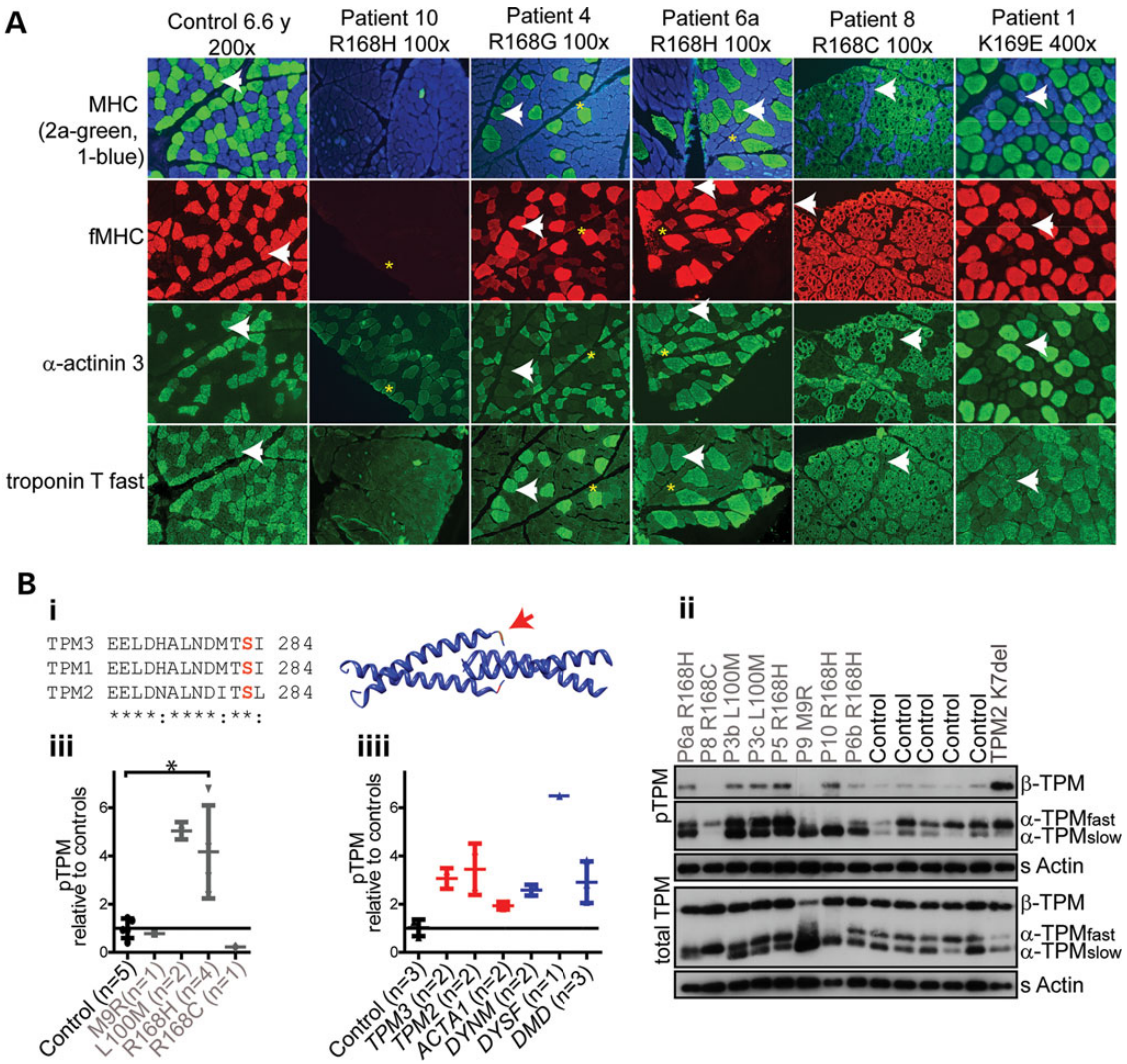

Figure 5. *TPM3* patients show increased phosphorylation of tropomyosin and ectopic expression of fast fibre specific α-actinin-3 in slow myofibres. (**A**) Consecutive sections were labelled with type-1 and type-2a MHC (blue and green, co-labelled respectively), type-2 MHC (red), α-actinin-3 (green) and troponin-T_{fast} (green) (the same fibre in multiple stains is indicated by a white arrow). Troponin-T_{fast} is only expressed in fast fibres as expected. Abnormal expression of α-actinin-3, a fast fibre specific Z-disc protein, was observed in type-1 myofibres of Patients 10, 4 and 6a (yellow stars). The biopsy of Patient 6b showed similar abnormalities but is not shown in this panel. Other patients had normal expression of α-actinin-3. Staining of Patient 1 and 8 are representative for these patients. (**Bi**) S283 is conserved and can be phosphorylated in all three sarcomeric tropomyosin proteins. (**Bii**) We assessed the level of S283 phosphorylation (pTPM) and total tropomyosin protein levels by duplicate western blot and equal loading was confirmed by using sarcomeric actin (s Actin) (representative western blot shown). The phosphorylation status of all three tropomyosin isoforms was determined by densitometry and normalized to the total tropomyosin levels. The graph shows phosphorylation levels normalized to the control average in (**Biii**) *TPM3* patients and (**Biiii**) patients with congenital myopathies and muscular dystrophies due to mutations in *TPM3*, *TPM2*, *ACTA1*, *DNM2*, *DMD* and *DYSF*. Horizontal lines and error bars represent mean and standard deviation. Phosphorylation was commonly increased in both *TPM3* patients and patients with other genetic causes of muscle disease. Statistical analysis was only performed on patients with the R168H mutation due to insufficient data points for other groups. Phosphorylation was significantly higher in patients with the R168H mutation compared with controls (*$P < 0.05$, Mann–Whitney *U* test).

Ca^{2+}-sensitivity of contraction and maximal contractile force are decreased in patients with TPM3 mutations

Tropomyosin and the troponin complex are pivotal in regulating Ca^{2+}-induced cross-bridge cycling during muscle contraction. We assessed the sensitivity to Ca^{2+} of permeabilised fibres, by bathing preparations in incrementally increasing [Ca^{2+}] (pCa 6.2-4.5) and measuring the generated contractile force. In slow myofibres and fibre bundles/hybrid fibres of all patients, the force-pCa curves were shifted to the right compared with controls (Fig. 8Ai–ii). As a result, the pCa_{50}, representing the negative logarithm of the [Ca^{2+}] at which preparations produce 50% of their Fmax, was significantly reduced in type-1 fibres and bundles/hybrid fibres from all patients compared with controls (pCa_{50} type-1: 5.96 ± 0.06 controls, 5.69 ± 0.04 patients; pCa_{50} bundles/hybrid: 5.99 ± 0.09 controls, 5.67 ± 0.05 patient, Fig. 8Bi–ii). This result indicates that more Ca^{2+} was required in patient biopsies than control biopsies to achieve the same relative force. In contrast, fast fibres from patients and controls showed normal Ca^{2+}-activated force production (Fig. 8Aiii and Biii).

Our data demonstrate that slow fibres and in bundles/hybrid fibres from patients with *TPM3* mutations produce on average ~ 63% of the force produced by control fibres at saturating [Ca^{2+}] (pCA 4.5). During a maximal contraction the intracellular [Ca^{2+}] can rise from resting levels of ~0.1 μM (pCa 7) to ~10 μM (pCa 5) (33). However, myofibres *in vivo* rarely undergo maximal stimulation

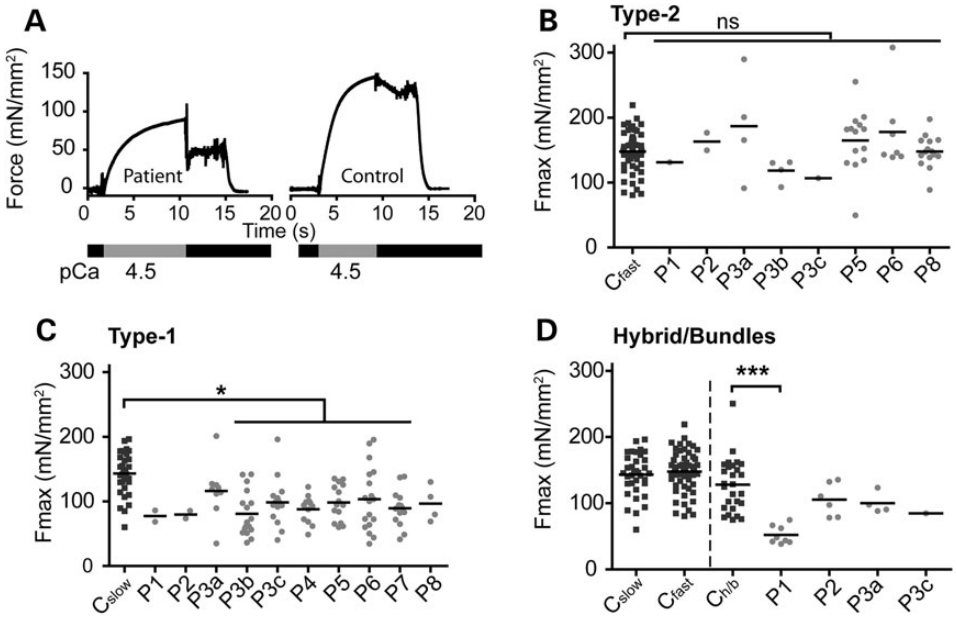

Figure 6. The force generation at saturating [Ca^{2+}] is decreased in *TPM3*-myopathy patients. Maximal force generation (Fmax) measured at pCa 4.5 and sarcomere length of 2.5 µm, normalized to fibre CSA. (**A**) A typical force trace from a patient (Patient 6) and control type-1 fibre. Most *TPM3* patients showed a significant force deficit in type-1 myofibres (**C**) whereas type-2 fibres produced similar maximal force compared with controls (**B**). In hybrid fibres and fibre bundles all patients had a slightly lower force average, however only Patient 1 showed a significant force deficit (**D**). C_{slow} = Control type-1 fibres (pooled from eight biopsies aged: 11–54 years), C_{fast} = Control type-2 fibres (pooled from eight biopsies aged: 6–54 years), $C_{h/b}$ = Control hybrid fibres (contain a mix of type-1 and type-2 MHC, age 11–54 years) and small fibre bundles (bundles were taken from two biopsies of 0.9- and 6-year-old controls). P = Patient. The black line in (B–D) indicates the average. $^{***}P < 0.0001$, $^{*}P < 0.01$, one-way ANOVA.

and mostly operate at sub-maximal levels, typically resulting in [Ca^{2+}] of around 1–5 µM) in type-1 fibres (yellow area in Fig. 8A) (34–36). At these physiological Ca^{2+} levels (pCa 6.0), slow fibres and bundles/hybrid fibres from *TPM3* patients produce on average only 26% of the force produced by control slow fibres and bundles/hybrid fibres (Fig. 8Ci–ii), whereas patient fast fibres produce forces similar to controls (Fig. 8Ciii). Thus, our results suggest reduced Ca^{2+}-sensitivity is a significant basis for muscle weakness in *TPM3*-myopathy.

Ectopic α-actinin-3 expression in slow myofibres does not correlate with increased maximal force

Four patients with *TPM3* mutations at R168 displayed ectopic expression of α-actinin-3 in slow myofibres. Since α-actinin-3 expression is associated with increased muscle strength and speed (26,27) we determined whether α-actinin-3 in slow fibres may influence contractile properties. We tested if α-actinin-3 expression was more commonly observed in fibres with higher Fmax in eight fibres from two patients. However, we found no correlation between ectopic α-actinin-3 and force production in these patient fibres (Supplementary Material, Fig. S5).

Discussion

Mutations in *TPM3* cause a range of histopathological patterns and are associated with generalized muscle weakness. To date, the cause of muscle dysfunction is not well understood in these patients, hindering the development of evidence-based treatments for *TPM3*-myopathies. Thus, we performed extensive phenotypical and functional characterization of a large cohort of *TPM3*-myopathy patients to understand the molecular mechanism(s) of their muscle weakness.

The main histological feature of *TPM3*-myopathy patients in this cohort, and other published cohorts (1–3), was a selective hypotrophy of slow myofibres, while other histological features such as nemaline rods and caps were rarely present (4 of 15 patients). The selective hypotrophy and contractile dysfunction of slow myofibres is consistent with the restricted slow-fibre expression of α-TPM_{slow}, the main protein expressed from *TPM3* in skeletal muscle. We confirmed the presence of mutant α-TPM_{slow} in the filamentous fraction of patient skeletal muscle via 2D-SDS-PAGE for patients possessing a *TPM3* mutation resulting in a charge change. In patients with protein aggregates (e.g. nemaline bodies), it has been uncertain whether mutant protein is actually incorporated into the sarcomere, or partitions into protein aggregates within the muscle fibre. In our study, protein aggregates were not observed in biopsies analysed by 2D-SDS-PAGE, suggesting that α-TPM_{slow} mutant protein is likely incorporated into sarcomeres causing muscle weakness via a dominant negative effect on contractile function. Interestingly, the amount of α-TPM_{slow} mutant protein did not correlate well with disease severity in our patient cohort. This may be explained by a number of factors influencing disease severity, such as a mutation-specific effect and varying proportions of slow fibres in different parts of the same muscle or different muscle groups.

Muscle contraction and force production rely on efficient interactions between tropomyosin polymers and major binding partners, the troponins and the actin filament, in response to Ca^{2+}-influx. In this series of 12 muscle biopsies from *TPM3*-myopathy patients, we showed normal fibre-type expression of the major contractile proteins myosin, actin, troponin and tropomyosin. Furthermore, we confirmed normal ratios of the three skeletal muscle tropomyosin isoforms according to fibre-type composition for all patients. Our data suggest the higher relative abundance of α-TPM_{slow} previously reported in a patient bearing a M9R substitution in *TPM3* (25,37) may be a specific property of

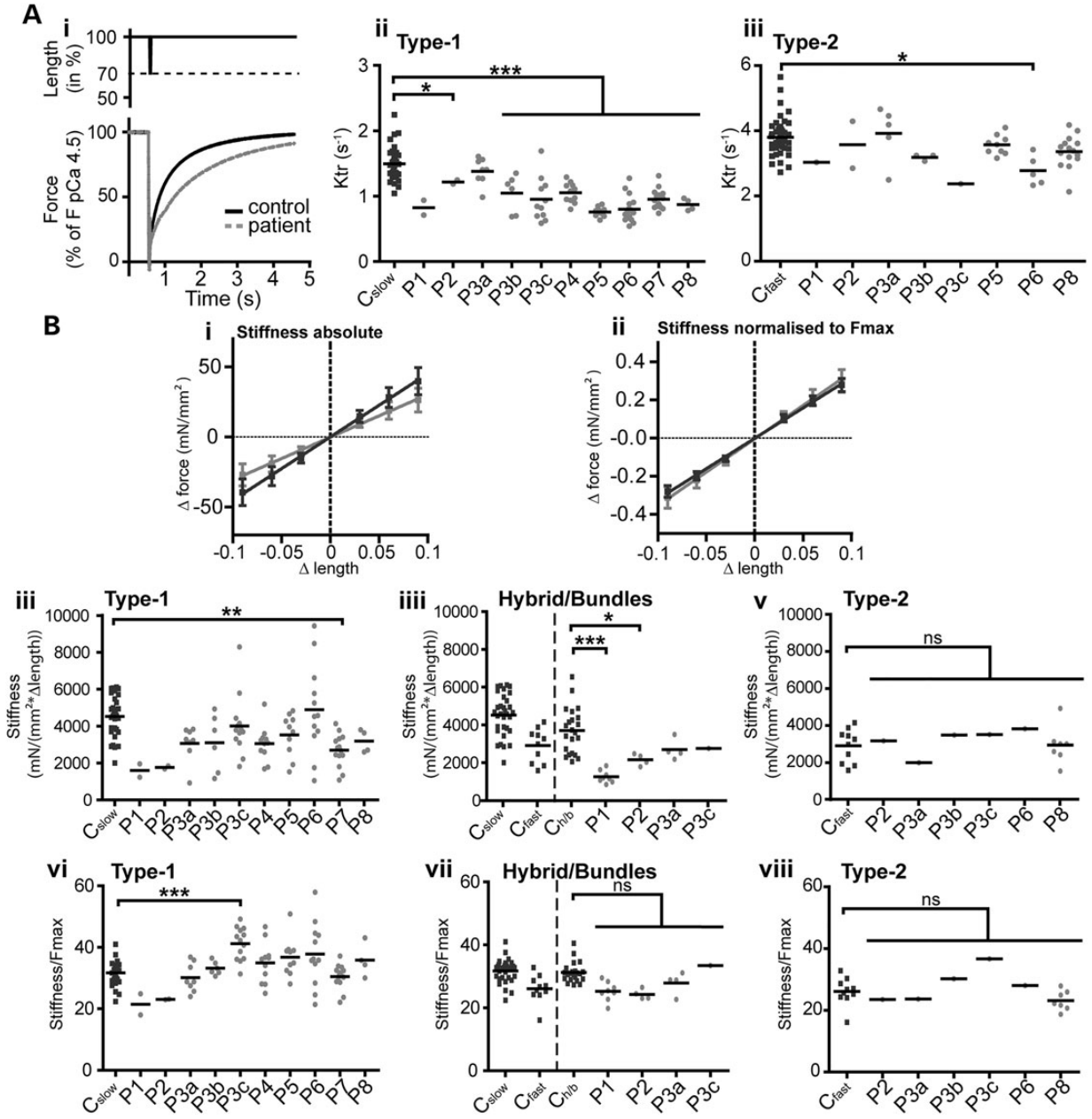

Figure 7. The force deficit in *TPM3*-myopathy patients is likely due to abnormal cross-bridge cycling. We assessed the rate of tension re-development (K_{tr}) (**A**) and active stiffness (**B**) in *TPM3*-myopathy patients to investigate if the force deficit in patient type-1 fibres was due to altered cross-bridge cycling. A typical K_{tr} trace of a patient (Patient 6) and a control are shown in (**Ai**). The K_{tr} in single myofibres from *TPM3* patient biopsies and control biopsies are shown in (**Aii**) (type-1) and (**Aiii**) (type-2). Note that due to different MHC-ATPase properties the K_{tr} is physiologically higher in type-2 than in type-1 fibres. (Aii) The type-1 fibres of most *TPM3* patients showed a significant decrease in K_{tr} compared with control type-1 fibres (exceptions: Patient 1, 2 and 3a) (***$P < 0.0001$, *$P < 0.01$, one-way ANOVA). (Aiii) The type-2 fibres were not different to control type-2 fibres, with the exception of Patient 6 which showed a small decrease in K_{tr}. (B) Active stiffness was analysed by plotting the length changes (ΔL) against the force changes (ΔF) and fitting a linear regression to the data. A representative graph of type-1 fibres from Patient 4 and from controls is shown in (**Bi**: absolute length change) and (**Bii**: length change/Fmax). Graphs from other all other samples are presented in Supplementary Material, Figure S6. Error bars represent standard deviation. (**Biii–v**) The slope of the linear regression was not significantly different from controls in all fibre types in most patients with the exception of type-1 fibres or bundles/hybrid fibres of Patient 1, 2 and 7 where stiffness was reduced (*$P < 0.01$, **$P < 0.001$, ***$P < 0.0001$, one-way ANOVA). However, a trend towards a small reduction was present in type-1 fibres and bundles/hybrid fibres of most patients (Biii-iii). (**vi** and **vii**) When ΔF was normalized to Fmax the slope was not significantly different from controls with the exception of P3c, which showed an increase in the slope (I, ***$P < 0.0001$, one-way ANOVA). Error bars represent standard deviation. C_{slow} and C_{fast} = Control type-1 and type-2 fibres (pooled from eight biopsies aged: 11–54 years), $C_{h/b}$ = Control hybrid fibres (contain a mix of type-1 and type-2 MHC, age 6–54 years) and small fibre bundles (bundles were taken from two biopsies of 0.9- and 6-year-old controls). The black line in all scatter plots indicates the average.

this mutation, perhaps related to its position within the dimerization domain. In a small number of patients, we observed ectopic expression of the fast fibre Z-disc protein α-actinin-3 in slow myofibres. The consequence of slow-fibre expression of the fast-fibre α-actinin-3 is not clear, and may relate to both metabolic and structural roles of α-actinin-3, though we excluded

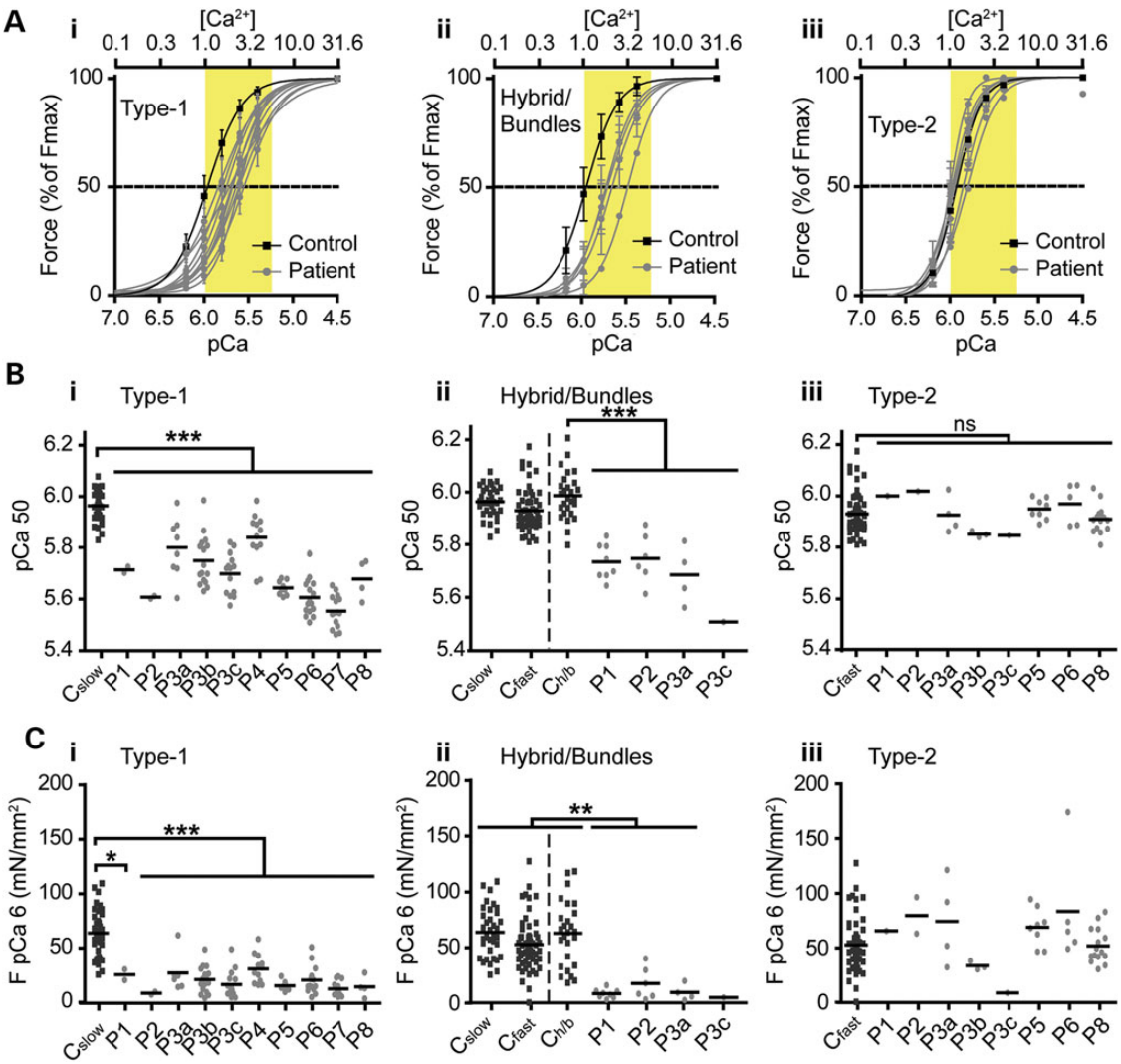

Figure 8. Ca^{2+}-sensitivity is decreased in *TPM3*-myopathy patients resulting in reduced specific force generation at physiological $[Ca^{2+}]$. (**A**) Specific force generation at incremental $[Ca^{2+}]$ in skinned type-1 fibres (**i**), hybrid fibres or bundles (**ii**) and type-2 fibres (**C**) shown as per cent of Fmax fitted to a variable slope log (dose) response curve. Note the rightward shift of the force/pCa curve in type-1 fibres, hybrid fibres/bundles in *TPM3* patients, whereas type-2 fibres were not different to controls. The dotted lines indicate the pCa50 ($[Ca^{2+}]$ required to achieve 50% of maximal force) and the yellow area indicates physiological cytoplasmic $[Ca^{2+}]$ during muscle contraction (between 1 and 5 μM). (**B**) The pCa 50 was significantly higher in type-1 fibres, hybrid fibres/bundles of *TPM3* patients compared with controls and type-2 fibres of *TPM3* patients. (C) Specific force generation measured at pCa 6.0 (1 μM, physiological calcium). The force was significantly lower in (**i**) type-1 fibres and (**ii**) hybrid fibres/bundles of all *TPM3* patients, but was not different from controls in (**iii**) type-2 fibres. C_{slow} and C_{fast} = Control type-1 and type-2 fibres (pooled from eight biopsies aged: 11–54 years), $C_{h/b}$ = Control hybrid fibres (contain a mix of type-1 and type-2 MHC, age 6–54 years) and small fibre bundles (bundles were taken from two biopsies of 0.9- and 6-year-old controls). The black line in the scatter plot indicates the average and error bars in force/pCa curves are standard deviations. ***$P < 0.0001$, *$P < 0.01$, one-way ANOVA. P = Patient, C = control.

an overt effect on contractile force of single myofibres. Interestingly, similar ectopic expression of α-actinin-3 was previously observed in some patients with *ACTA1* mutations (38) and is thus not specific to *TPM3*-associated disease but could potentially be due to incomplete or abnormal fibre type conversion present in some myopathy patients.

We investigated tropomyosin phosphorylation at residue S283 in our cohort. Tropomyosin phosphorylation has mainly been studied in the context of cardiac function (39–42) and to the best of our knowledge has not been investigated in skeletal myopathy patients. *In vitro* studies suggest phosphorylation strongly affects tropomyosin properties [e.g. stronger head-to-tail interaction, enhanced troponin binding, higher myosin ATPase activity and long-range cooperative activation of myosin-thin filament binding (30,43,44)]. We showed tropomyosin phosphorylation was commonly increased in a wide range of genetic muscle disorders including *TPM3*-myopathy. However, the cause of this up-regulation and the effect on skeletal muscle contractility is unclear. The p38-MAPK (mitogene-activated protein kinase) and ERK (extracellular signal-related kinase) signalling pathways are likely involved in tropomyosin phosphorylation of cardiac muscle and non-muscle cells, respectively (45–47). In skeletal muscle, these pathways regulate exercise-induced adaptive responses on gene expression (reviewed in 48), suggesting tropomyosin phosphorylation may be involved in remodelling or adaptation to cellular stress.

Most reported *TPM3* substitutions lie within or near actin-binding domains, with several substitutions believed to influence direct electrostatic interactions with actin in the 'off' state [when tropomyosin blocks myosin binding sites on the actin filament,

e.g. R91, R168, R245 directly interact with actin D25 (49–51)]. Our data and previous studies have shown that many tropomyosin substitutions indeed affect binding to actin-filaments (52–55). Thus, altered actin-binding likely represents a common mechanism by which tropomyosin mutants alter sarcomeric function, perhaps related to the Ca^{2+}-activated movement of tropomyosin between the 'on' and 'off' position during cross-bridge cycling (51, discussed in 56).

Recent studies have attempted to predict the effect of mutations on actin–tropomyosin interactions and the resulting contractile abnormality, classifying them as 'gain-of-function' changes (hyper-contractile phenotype, shift towards 'on' state) and 'loss-of-function' changes (hypo-contractile phenotype, stabilizing the 'off' state) (50,57,58). Most mutations in our cohort are predicted to cause a 'loss-of-function' (e.g. decreased Ca^{2+}-sensitivity and a hypocontractile phenotype). The only exception is *TPM3* K169E, predicted to favour the 'on' position and enhance myosin-actin binding (50,57). This phenotype was confirmed in reconstituted thin filaments *in vitro* (50). However, isolated slow myofibres and fibre bundles of all *TPM3* patients (including Patient 1 carrying the K169E mutation), showed reduced Ca^{2+}-sensitivity of contraction. Our data are consistent with the patient phenotype described in (1) and do not support the hyper-contractile phenotype of the K169E mutation present in *in vitro* assessment of isolated filaments (50). This discrepancy may be explained by the greater complexity of single-fibre contractility studies, a setting that evaluates the combined contributions of actin, tropomyosin and troponin binding and regulatory proteins within a mature myofibre, which may also have undergone adaptive responses to disease. These may not be mirrored by *in vitro* actin motility studies or predictions via molecular modelling. Additional factors, such as interactions with other sarcomeric proteins like the troponin complex (59), may also contribute. Additionally, a recurrent mutation in *TPM3*, R168H, was found to reduce [current study and (22)] or increase Ca^{2+}-sensitivity (21) in different patients with the same mutation. The cause for this patient to patient variability remains to be established.

In our study, we identified two major abnormalities in contractile performance that we believe directly underpins weakness in *TPM3*-myopathy. Firstly, all patients exhibited reduced Ca^{2+}-sensitivity of contraction in slow myofibres, likely resulting in a significant reduction in the contractile force generated at physiological, sub-maximal activation of muscle. Secondly, slow myofibres demonstrated a significant reduction in cross-bridge cycling kinetics and a small reduction in active stiffness (assesses the number of strongly bound myosin-actin cross-bridges)—meaning that myosin less effectively and less stably transits along actin filaments during contraction. Collectively, these two abnormalities likely cause insufficient force production during a normal action potential resulting in slow fibre weakness.

The selective dysfunction of slow myofibres in our cohort demonstrates the importance of assessing the two fibre types separately, and raises the question as to why fast myofibres are not able to compensate for dysfunctional slow myofibres. Inherent differences exist between the two fibre types. Slow myofibres are less fatigable than fast myofibres, probably due at least in part to larger numbers of mitochondria and a greater capacity for oxidative metabolism (60,61). Additionally, fast myofibres have a higher ATP consumption. Particular muscle groups, such as respiratory muscles, rely on slow fibres to produce sustained, low intensity contractions. Substantial weakness of respiratory muscles is common in *TPM3* patients, and effective treatments that specifically target slow muscle fibre dysfunction may ameliorate respiratory insufficiency.

In summary, contractile function was commonly impaired in *TPM3*-myopathy patients. In particular, we showed reduced force generation caused by altered cross-bridge cycling kinetics and reduced Ca^{2+}-sensitivity of muscle contraction. The identification of abnormal Ca^{2+}-sensitivity suggests the use of Ca^{2+}-sensitisers may present a viable therapeutic approach for TPM-related myopathies. To date, a number of agents are known to be effective at improving Ca^{2+}-sensitivity in isolated skeletal myofibres from various species including bovine, human, mouse and rabbit (22,62–65). Additionally, Ca^{2+}-sensitisers were able to ameliorate muscle dysfunction in a rat model of myasthenia gravis (62) and isolated skeletal myofibres from congenital myopathy patients with mutations in *TPM3*, *TPM2* and *NEB* (22,63). This therapeutic approach appears to be promising; however, most of these agents target the fast troponin isoforms and are unlikely to ameliorate slow fibre dysfunction. A Ca^{2+}-sensitiser acting on slow skeletal/cardiac troponin-C did not improve Ca^{2+}-sensitivity in skeletal myofibres in a recent study, suggesting that new compounds targeting slow myofibre dysfunction have yet to be developed (66). Also, it appears that *TPM2* and *TPM3* mutations can either increase or decrease Ca^{2+}-sensitivity in a patient and mutation-specific manner (overview in Supplementary Material, Table S4), thus Ca^{2+}-sensitisers will only be useful in a subset of patients. Patients with increased Ca^{2+}-sensitivity display a hyper-contractile clinical phenotype (22,54), suggesting treatment with Ca^{2+}-sensitisers must be tightly regulated to ensure appropriate muscle function and avoid side effects.

Materials and Methods

Study approval

This study was approved by the human ethics committees of the Stollery Children's Hospital, Edmonton, Canada (ID: 5856), Royal Children's Hospital, Melbourne, Australia (ID: 21102A), Children's Hospital at Westmead, Sydney, Australia (ID: 2000/068, 10. CHW.45), University of Sydney, Australia (ID: 01/11/50) and Boston Children's Hospital Institutional Review Board (03-08-128R). Informed consent was obtained from all individuals.

Molecular modelling

Molecular modelling was based on the 7 Ångstroms resolution crystal structure of an α-TPM_{fast} dimer isolated from adult porcine ventricles [RCSB Protein Data Bank 1C1G, Whitby and Phillips (18)]. Molecular graphics were created with Swiss-PDB Viewer v4.1.0 (19).

Antibodies

Mouse anti-sarcomeric actin (5C5, 1:100 for IHC and 1:10 000 for western blot), fast myosin (MY32, 1:800 for IHC), tropomyosin (TM311, 1:20 000 for western blot and 1:800 for IHC), troponin-T_{fast} (TNNT3, 1:30 for IHC and 1:1000 for western blot) were obtained from Sigma Aldrich. S283-phosphorylated tropomyosin was detected using the rabbit anti-Tm-pS283-050 (1:500 for western blot and 1:30 for IHC, 21st Century Biochemicals) and slow myosin antibodies were obtained from Chemicon (1:800 for IHC and 1:7000 for western blot). Polyclonal α-actinin-3 antibodies were produced in-house (antibody 5B3 diluted 1:50 for IHC and antibody 5A2 1:1500 for western blot) (67). Troponin-I_{slow} (MYNT-S, diluted 1:10 for IHC) and fast (MYNT-F, diluted 1:150) antibodies were kindly supplied by Takeshi Nakamura, Japan.

Troponin-T_{slow} antibodies (CT3) were obtained from the Developmental Studies Hybridoma Bank, University of Iowa (diluted 1:50 for IHC). Cardiac actin and neonatal MHC antibodies were obtained from American Research Products Inc., USA and Novocastra Laboratories Ltd, UK, respectively.

IHC and Zenon labelling

IHC was performed as described previously (68). Sections were either fixed as described in (37) (MYNT-S) or for 10 min in 3% PFA (MYNT-F, CT3 and TNNT3) or used unfixed (other antibodies). A Zenon mouse IgG labelling kit (Molecular Probes) was used to directly label primary antibodies with different fluorophores for co-staining with two mouse antibodies as per manufacturer's instructions [either MHC type-2A and type-1 (Fig. 5) or neonatal MHC and cardiac actin (Supplementary Material, Fig. S2C)]. Staining was imaged using standard fluorescence microscopy.

Fibre morphometry

Fibre morphometry was performed on cryo-sections stained for myosin ATPase (69) or following IHC for MHC isoforms. At least 200 fibres, visible in two distant fields of the same section were analysed using ImagePro Plus 4 software (Media Cybernetics). The greatest distance between opposite sides of the narrowest aspect, the MinFeret diameter, was measured to obtain the fibre diameter from a cross sectional cut. The %FSD was calculated as described in (1) and slow fibre area was calculated assuming circular shape of myofibres.

Western blot and 2D-SDS-PAGE

Western blot methods were based on (70) and tropomyosin isoforms were resolved as described in (54). Extraction of the filamentous protein pool from skeletal muscle sections and 2D-SDS-PAGE to determine mutant tropomyosin expression were performed as described previously (13,71).

Protein sources and actin-tropomyosin co-sedimentation

We employed site-directed mutagenesis to produce wild-type and mutant (R168C, K169E) α-TPM_{slow} baculoviruses to infect *Sf*9 insect cells using the baculovirus expression method as described previously (55,72).

Filamentous actin was prepared from actin-acetone powder isolated from rabbit muscle (73) and a 1 μM stock with 1 μM phalloidin and 0.1 mM ATP was used for experiments.

All protein stocks were prepared in and dialysed against a buffer containing 100 mM KCl, 50 mM Imidazole, 8 mM $MgCl_2$, 2 mM EDTA, 10 mM DTT and 0.5 mg/mL ultrapure bovine serum albumin (Sigma). Ten μM tropomyosin stocks were cleared of aggregates by ultracentrifugation at 603 180*g* (Sorvall M120-SE centrifuge, S100AT6-0199 rotor) for 20 min at 4°C. Ten nM actin were co-sedimented with incremental amounts of tropomyosin (50–1000 nM) in 1 ml reaction volume at 51 427*g* for 1.5 h at 25°C (Sorvall Evolution RC centrifuge, F20-Micro rotor) in siliconised polypropylene tubes. The pelleted fractions were solubilized in loading buffer and loaded on 4–15% Criterion TGX gels (Biorad). Densitometry analysis on actin and tropomyosin bands was performed using GeneTools 4.0 software (Synoptics Ltd). Values were corrected for sedimentation in the absence of actin and plotted as the ratio tropomyosin/actin versus. total [tropomyosin] added. Data were fitted to a Hill equation to determine the binding constant K_d and Hill's coefficient h using GraphPad, Prism (Version 5.01).

Contractile measurement of myofibres isolated from frozen human muscle biopsies

Small fractions of frozen muscle biopsies were thawed as described previously (63) in a solution containing 50% glycerol and 50% Ca^{2+}-free relaxing-solution (100 mM BES, 6.97 mM EGTA, 6.48 mM $MgCl_2$, 6 mM Na_2ATP, 1 mM DTT, 40.76 mM K-propionate, 14.5 mM creatine phosphate, 0.5 mM PMSF, 10 μM E64, 40 μM leupeptin, pH 7.1 and pCa 9 at 15°C).

For contractile measurements, single fibres or small fibre bundles [~0.07 mm^2 CSA and ~0.5 mm length] were dissected in glycerinating solution at 4°C. Fibre bundles were prepared if the fibre CSA was too small for reliable force measurements. Aluminium T-clips were attached to both ends of the preparation followed by chemical skinning in glycerinating solution containing 1% Triton X-100 for 10 min (single fibres) or 30 min (bundles) at 4°C. The preparations were then stored at 4°C in glycerinating solution until mounting onto a permeabilised fibre apparatus between a length motor and a force transducer (ASI 802D, ASI 403A, ASI 315C-I, respectively, Aurora Scientific Inc., Canada) in relaxing-solution. All force measurements were performed at sarcomere lengths of 2.5 μm [optimal myofilament overlap (74)] and at a temperature of 20°C (bath temperature controller ASI 825A, Aurora Scientific). The sarcomere length was set and the CSA was measured as described in (63).

Prior to $[Ca^{2+}]$-induced activations preparations were pre-activated for 1 min in 100 mM BES, 0.1 mM EGTA, 6.42 mM $MgCl_2$, 6 mM Na_2ATP, 41.14 mM K-propionate, 14.5 mM creatine phosphate, 6.9 mM HDTA (pH 7.1 and pCa 9 at 15°C). Maximal isometric contraction (Fmax) was measured by bathing fibres in saturating $[Ca^{2+}]$ buffer (100 mM BES, 7 mM CaEGTA, 6.28 mM $MgCl_2$, 6 mM Na_2ATP, 40.64 mM K-propionate, 14.5 mM creatine phosphate, pH 7.1 and pCa 4.5 at 15°C) until a force plateau was achieved. The maximal specific force (Fmax at pCa 4.5 normalized to the CSA) is presented in this study. Force/pCa curves and pCa 50 were measured as described in (21). The rate constant of tension re-development (K_{tr}) was measured by allowing the preparations to shorten to 70% of the initial length for 30 ms followed by re-stretch to 100% and fitting the data to a mono-exponential function using Labview (National Instruments, USA) as described in (21). Active stiffness was measured immediately after the K_{tr} protocol as described previously (32,75). In brief, we measured the force response (*F1*) to six 2 s length changes (ΔL: +0.3%, +0.6%, +0.9%, −0.3%, −0.6%, −0.9%; Supplementary Material, Fig. S4). ΔL was plotted against the force changes (ΔF) and a linear regression was fitted to obtain the slope using Graph Pad, Prism (Version 5.01).

The MHC content of measured fibres was determined as described previously (63) and the proportion of each MHC was determined by densitometry. Single myofibres/fibre bundles containing exclusively slow MHC (>90% type-1), exclusively fast MHC (>90% type-2A or 2X) or a mixture of both (11–90% type-1 or type-2A/2X) were grouped for analysis. The contractile properties of bundles and hybrid fibres containing a mix of type-1 and type-2A/2X MHC represent the average properties of both fibre types. The K_{tr} in bundles/hybrid fibres is highly variable due to the physiologically difference in type-1 or type-2A/2X fibres and was therefore not presented. Preparations were excluded from the analysis if the Fmax decreased >15% during the protocol. Single myofibres from eight control biopsies (age 6–54 years) and bundles from two control biopsies (aged 0.6 and 6 years) were pooled for statistical analysis.

Supplementary Material

Supplementary Material is available at *HMG* online.

Acknowledgements

The authors thank the study patients and their families for their participation. Additionally, we are thankful to Dr Nicole Monnier and Dr Isabelle Pennison-Besnier (CHU Angers, Département de Neurologie, Angers, France) for supply patient tissue for this study.

Conflict of Interest statement. None declared.

Funding

This work was supported by the National Health and Medical Research Council of Australia (APP571287 to N.F.C., K.N.N. and B.I.; APP1022707 to N.F.C. and K.N.N.; APP1048816 to S.T.C.; APP1035955 to G.R.) and by the National Institutes of Health (USA) (R01 HD075802 from the National Institute of Child Health and Human Development to A.H.B.). M.Y. is supported by a University of Sydney Australian Postgraduate Award, an International Postgraduate Research Scholarship and a Boehringer Ingelheim Fonds Travel Grant. K.J.N. is supported by an Australian Resource Council Future Fellowship (FT100100734).

References

1. Clarke, N.F., Kolski, H., Dye, D.E., Lim, E., Smith, R.L., Patel, R., Fahey, M.C., Bellance, R., Romero, N.B., Johnson, E.S. *et al.* (2008) Mutations in TPM3 are a common cause of congenital fiber type disproportion. *Ann. Neurol.*, **63**, 329–337.
2. Lawlor, M.W., Dechene, E.T., Roumm, E., Geggel, A.S., Moghadaszadeh, B. and Beggs, A.H. (2010) Mutations of tropomyosin 3 (TPM3) are common and associated with type 1 myofiber hypotrophy in congenital fiber type disproportion. *Hum. Mutat.*, **31**, 176–183.
3. Marttila, M., Lehtokari, V.L., Marston, S., Nyman, T.A., Barnerias, C., Beggs, A.H., Bertini, E., Ceyhan-Birsoy, O., Cintas, P., Gerard, M. *et al.* (2014) Mutation update and genotype-phenotype correlations of novel and previously described mutations in TPM2 and TPM3 causing congenital myopathies. *Hum. Mutat.*, **35**, 779–790.
4. Tan, P., Briner, J., Boltshauser, E., Davis, M.R., Wilton, S.D., North, K., Wallgren-Pettersson, C. and Laing, N.G. (1999) Homozygosity for a nonsense mutation in the alpha-tropomyosin slow gene TPM3 in a patient with severe infantile nemaline myopathy. *Neuromuscul. Disord.*, **9**, 573–579.
5. Wattanasirichaigoon, D., Swoboda, K.J., Takada, F., Tong, H. Q., Lip, V., Iannaccone, S.T., Wallgren-Pettersson, C., Laing, N.G. and Beggs, A.H. (2002) Mutations of the slow muscle alpha-tropomyosin gene, TPM3, are a rare cause of nemaline myopathy. *Neurology*, **59**, 613–617.
6. Lehtokari, V.-L., Pelin, K., Donner, K., Voit, T., Rudnik-Schöneborn, S., Stoetter, M., Talim, B., Topaloglu, H., Laing, N.G. and Wallgren-Pettersson, C. (2008) Identification of a founder mutation in TPM3 in nemaline myopathy patients of Turkish origin. *Eur. J. Hum. Genet.*, **16**, 1055–1061.
7. Laing, N.G., Wilton, S.D., Akkari, P.A., Dorosz, S., Boundy, K., Kneebone, C., Blumbergs, P., White, S., Watkins, H., Love, D. R. *et al.* (1995) A mutation in the alpha tropomyosin gene TPM3 associated with autosomal dominant nemaline myopathy. *Nat. Genet.*, **9**, 75–79.
8. Schreckenbach, T., Schroder, J.M., Voit, T., Abicht, A., Neuen-Jacob, E., Roos, A., Bulst, S., Kuhl, C., Schulz, J.B., Weis, J. *et al.* (2014) Novel TPM3 mutation in a family with cap myopathy and review of the literature. *Neuromuscul. Disord.*, **24**, 117–124.
9. Kiphuth, I.C., Krause, S., Huttner, H.B., Dekomien, G., Struffert, T. and Schroder, R. (2010) Autosomal dominant nemaline myopathy caused by a novel alpha-tropomyosin 3 mutation. *J. Neurol.*, **257**, 658–660.
10. Ohlsson, M., Fidzianska, A., Tajsharghi, H. and Oldfors, A. (2009) TPM3 mutation in one of the original cases of cap disease. *Neurology*, **72**, 1961–1963.
11. De Paula, A.M., Franques, J., Fernandez, C., Monnier, N., Lunardi, J., Pellissier, J.F., Figarella-Branger, D. and Pouget, J. (2009) A TPM3 mutation causing cap myopathy. *Neuromuscul. Disord.*, **19**, 685–688.
12. Penisson-Besnier, I., Monnier, N., Toutain, A., Dubas, F. and Laing, N. (2007) A second pedigree with autosomal dominant nemaline myopathy caused by TPM3 mutation: a clinical and pathological study. *Neuromuscul. Disord.*, **17**, 330–337.
13. Waddell, L.B., Kreissl, M., Kornberg, A., Kennedy, P., McLean, C., Labarre-Vila, A., Monnier, N., North, K.N. and Clarke, N.F. (2010) Evidence for a dominant negative disease mechanism in cap myopathy due to TPM3. *Neuromuscul. Disord.*, **20**, 464–466.
14. Geeves, M.A., Hitchcock-DeGregori, S.E. and Gunning, P.W. (2015) A systematic nomenclature for mammalian tropomyosin isoforms. *J. Muscle Res. Cell Motil.*, **36**, 147–153.
15. Billeter, R., Heizmann, C.W., Reist, U., Howald, H. and Jenny, E. (1981) alpha- and beta-tropomyosin in typed single fibers of human skeletal muscle. *FEBS Lett.*, **132**, 133–136.
16. Pieples, K. and Wieczorek, D.F. (2000) Tropomyosin 3 increases striated muscle isoform diversity. *Biochemistry (Mosc)*, **39**, 8291–8297.
17. McLachlan, A.D. and Stewart, M. (1975) Tropomyosin coiled-coil interactions: evidence for an unstaggered structure. *J. Mol. Biol.*, **98**, 293–304.
18. Polgar, J., Johnson, M.A., Weightman, D. and Appleton, D. (1973) Data on fibre size in thirty-six human muscles. An autopsy study. *J. Neurol. Sci.*, **19**, 307–318.
19. Guex, N. and Peitsch, M.C. (1997) SWISS-MODEL and the Swiss-PdbViewer: an environment for comparative protein modeling. *Electrophoresis*, **18**, 2714–2723.
20. McLachlan, A.D. and Stewart, M. (1976) The 14-fold periodicity in alpha-tropomyosin and the interaction with actin. *J. Mol. Biol.*, **103**, 271–298.
21. Ottenheijm, C.A., Lawlor, M.W., Stienen, G.J., Granzier, H. and Beggs, A.H. (2011) Changes in cross-bridge cycling underlie muscle weakness in patients with tropomyosin 3-based myopathy. *Hum. Mol. Genet.*, **20**, 2015–2025.
22. Ochala, J., Gokhin, D.S., Penisson-Besnier, I., Quijano-Roy, S., Monnier, N., Lunardi, J., Romero, N.B. and Fowler, V.M. (2012) Congenital myopathy-causing tropomyosin mutations induce thin filament dysfunction via distinct physiological mechanisms. *Hum. Mol. Genet.*, **21**, 4473–4485.
23. Johnson, M.A., Polgar, J., Weightman, D. and Appleton, D. (1973) Data on the distribution of fibre types in thirty-six human muscles. An autopsy study. *J. Neurol. Sci.*, **18**, 111–129.
24. Billeter, R., Heizmann, C.W., Reist, U., Howald, H. and Jenny, E. (1982) Two-dimensional peptide analysis of myosin heavy chains and actin from single-typed human skeletal muscle fibers. *FEBS Lett.*, **139**, 45–48.
25. Corbett, M.A., Akkari, P.A., Domazetovska, A., Cooper, S.T., North, K.N., Laing, N.G., Gunning, P.W. and Hardeman, E.C. (2005) An alphaTropomyosin mutation alters dimer preference in nemaline myopathy. *Ann. Neurol.*, **57**, 42–49.
26. Clarkson, P.M., Devaney, J.M., Gordish-Dressman, H., Thompson, P.D., Hubal, M.J., Urso, M., Price, T.B., Angelopoulos, T.J., Gordon, P.M., Moyna, N.M. *et al.* (2005) ACTN3 genotype is

associated with increases in muscle strength in response to resistance training in women. *J. Appl. Physiol.*, **99**, 154–163.
27. Eynon, N., Hanson, E.D., Lucia, A., Houweling, P.J., Garton, F., North, K.N. and Bishop, D.J. (2013) Genes for elite power and sprint performance: ACTN3 leads the way. *Sports Med.*, **43**, 803–817.
28. Mak, A., Smillie, L.B. and Barany, M. (1978) Specific phosphorylation at serine-283 of alpha tropomyosin from frog skeletal and rabbit skeletal and cardiac muscle. *Proc. Natl Acad. Sci. USA*, **75**, 3588–3592.
29. Montarras, D., Fiszman, M.Y. and Gros, F. (1981) Characterization of the tropomyosin present in various chick embryo muscle types and in muscle cells differentiated in vitro. *J. Biol. Chem.*, **256**, 4081–4086.
30. Rao, V.S., Marongelli, E.N. and Guilford, W.H. (2009) Phosphorylation of tropomyosin extends cooperative binding of myosin beyond a single regulatory unit. *Cell Motil. Cytoskeleton*, **66**, 10–23.
31. Linari, M., Caremani, M., Piperio, C., Brandt, P. and Lombardi, V. (2007) Stiffness and fraction of Myosin motors responsible for active force in permeabilized muscle fibers from rabbit psoas. *Biophys. J.*, **92**, 2476–2490.
32. Chandra, M., Mamidi, R., Ford, S., Hidalgo, C., Witt, C., Ottenheijm, C., Labeit, S. and Granzier, H. (2009) Nebulin alters cross-bridge cycling kinetics and increases thin filament activation: a novel mechanism for increasing tension and reducing tension cost. *J. Biol. Chem.*, **284**, 30889–30896.
33. Baylor, S.M. and Hollingworth, S. (2012) Intracellular calcium movements during excitation-contraction coupling in mammalian slow-twitch and fast-twitch muscle fibers. *J. Gen. Physiol.*, **139**, 261–272.
34. Westerblad, H. and Allen, D.G. (1991) Changes of myoplasmic calcium concentration during fatigue in single mouse muscle fibers. *J. Gen. Physiol.*, **98**, 615–635.
35. Allen, D.G., Lamb, G.D. and Westerblad, H. (2008) Skeletal muscle fatigue: cellular mechanisms. *Physiol. Rev.*, **88**, 287–332.
36. Launikonis, B.S., Stephenson, D.G. and Friedrich, O. (2009) Rapid Ca2+ flux through the transverse tubular membrane, activated by individual action potentials in mammalian skeletal muscle. *J. Physiol.*, **587**, 2299–2312.
37. Ilkovski, B., Mokbel, N., Lewis, R.A., Walker, K., Nowak, K.J., Domazetovska, A., Laing, N.G., Fowler, V.M., North, K.N. and Cooper, S.T. (2008) Disease severity and thin filament regulation in M9R TPM3 nemaline myopathy. *J. Neuropathol. Exp. Neurol.*, **67**, 867–877.
38. Ilkovski, B., Cooper, S.T., Nowak, K., Ryan, M.M., Yang, N., Schnell, C., Durling, H.J., Roddick, L.G., Wilkinson, I., Kornberg, A.J. *et al.* (2001) Nemaline myopathy caused by mutations in the muscle alpha-skeletal-actin gene. *Am. J. Hum. Genet.*, **68**, 1333–1343.
39. Marston, S.B., Copeland, O., Messer, A.E., MacNamara, E., Nowak, K., Zampronio, C.G. and Ward, D.G. (2013) Tropomyosin isoform expression and phosphorylation in the human heart in health and disease. *J. Muscle Res. Cell Motil.*, **34**, 189–197.
40. Schulz, E.M., Wilder, T., Chowdhury, S.A., Sheikh, H.N., Wolska, B.M., Solaro, R.J. and Wieczorek, D.F. (2013) Decreasing tropomyosin phosphorylation rescues tropomyosin-induced familial hypertrophic cardiomyopathy. *J. Biol. Chem.*, **288**, 28925–28935.
41. Schulz, E.M. and Wieczorek, D.F. (2013) Tropomyosin dephosphorylation in the heart: what are the consequences? *J. Muscle Res. Cell Motil.*, **34**, 239–246.
42. Warren, C.M., Arteaga, G.M., Rajan, S., Ahmed, R.P., Wieczorek, D.F. and Solaro, R.J. (2008) Use of 2-D DIGE analysis reveals altered phosphorylation in a tropomyosin mutant (Glu54Lys) linked to dilated cardiomyopathy. *Proteomics*, **8**, 100–105.
43. Heeley, D.H. (2013) Phosphorylation of tropomyosin in striated muscle. *J. Muscle Res. Cell Motil.*, **34**, 233–237.
44. Lehman, W., Medlock, G., Li, X.E., Suphamungmee, W., Tu, A. Y., Schmidtmann, A., Ujfalusi, Z., Fischer, S., Moore, J.R., Geeves, M.A. *et al.* (2015) Phosphorylation of Ser283 enhances the stiffness of the tropomyosin head-to-tail overlap domain. *Arch. Biochem. Biophys.*, **571**, 10–15.
45. Vahebi, S., Ota, A., Li, M., Warren, C.M., de Tombe, P.P., Wang, Y. and Solaro, R.J. (2007) p38-MAPK induced dephosphorylation of alpha-tropomyosin is associated with depression of myocardial sarcomeric tension and ATPase activity. *Circ. Res.*, **100**, 408–415.
46. Houle, F., Poirier, A., Dumaresq, J. and Huot, J. (2007) DAP kinase mediates the phosphorylation of tropomyosin-1 downstream of the ERK pathway, which regulates the formation of stress fibers in response to oxidative stress. *J. Cell Sci.*, **120**, 3666–3677.
47. Houle, F., Rousseau, S., Morrice, N., Luc, M., Mongrain, S., Turner, C.E., Tanaka, S., Moreau, P. and Huot, J. (2003) Extracellular signal-regulated kinase mediates phosphorylation of tropomyosin-1 to promote cytoskeleton remodeling in response to oxidative stress: impact on membrane blebbing. *Mol. Biol. Cell*, **14**, 1418–1432.
48. Widegren, U., Ryder, J.W. and Zierath, J.R. (2001) Mitogen-activated protein kinase signal transduction in skeletal muscle: effects of exercise and muscle contraction. *Acta Physiol. Scand.*, **172**, 227–238.
49. Li, X.E., Tobacman, L.S., Mun, J.Y., Craig, R., Fischer, S. and Lehman, W. (2011) Tropomyosin position on F-actin revealed by EM reconstruction and computational chemistry. *Biophys. J.*, **100**, 1005–1013.
50. Marston, S., Memo, M., Messer, A., Papadaki, M., Nowak, K., McNamara, E., Ong, R., El-Mezgueldi, M., Li, X. and Lehman, W. (2013) Mutations in repeating structural motifs of tropomyosin cause gain of function in skeletal muscle myopathy patients. *Hum. Mol. Genet.*, **22**, 4978–4987.
51. Orzechowski, M., Moore, J.R., Fischer, S. and Lehman, W. (2014) Tropomyosin movement on F-actin during muscle activation explained by energy landscapes. *Arch. Biochem. Biophys.*, **545**, 63–68.
52. Robaszkiewicz, K., Dudek, E., Kasprzak, A.A. and Moraczewska, J. (2012) Functional effects of congenital myopathy-related mutations in gamma-tropomyosin gene. *Biochim. Biophys. Acta*, **1822**, 1562–1569.
53. Moraczewska, J., Greenfield, N.J., Liu, Y. and Hitchcock-DeGregori, S.E. (2000) Alteration of tropomyosin function and folding by a nemaline myopathy-causing mutation. *Biophys. J.*, **79**, 3217–3225.
54. Mokbel, N., Ilkovski, B., Kreissl, M., Memo, M., Jeffries, C.M., Marttila, M., Lehtokari, V.L., Lemola, E., Gronholm, M., Yang, N. *et al.* (2013) K7del is a common TPM2 gene mutation associated with nemaline myopathy and raised myofibre calcium sensitivity. *Brain*, **136**, 494–507.
55. Akkari, P.A., Song, Y., Hitchcock-DeGregori, S., Blechynden, L. and Laing, N. (2002) Expression and biological activity of Baculovirus generated wild-type human slow alpha tropomyosin and the Met9Arg mutant responsible for a dominant form of nemaline myopathy. *Biochem. Biophys. Res. Commun.*, **296**, 300–304.

56. Ochala, J. (2008) Thin filament proteins mutations associated with skeletal myopathies: defective regulation of muscle contraction. *J. Mol. Med.*, **86**, 1197–1204.
57. Memo, M. and Marston, S. (2013) Skeletal muscle myopathy mutations at the actin tropomyosin interface that cause gain- or loss-of-function. *J. Muscle Res. Cell Motil.*, **34**, 165–169.
58. Orzechowski, M., Fischer, S., Moore, J.R., Lehman, W. and Farman, G.P. (2014) Energy landscapes reveal the myopathic effects of tropomyosin mutations. *Arch. Biochem. Biophys.*, **564**, 89–99.
59. Robaszkiewicz, K., Ostrowska, Z., Cyranka-Czaja, A. and Moraczewska, J. (2015) Impaired tropomyosin-troponin interactions reduce activation of the actin thin filament. *Biochim. Biophys. Acta*, **1854**, 381–390.
60. Schwerzmann, K., Hoppeler, H., Kayar, S.R. and Weibel, E.R. (1989) Oxidative capacity of muscle and mitochondria: correlation of physiological, biochemical, and morphometric characteristics. *Proc. Natl Acad. Sci. USA*, **86**, 1583–1587.
61. Jackman, M.R. and Willis, W.T. (1996) Characteristics of mitochondria isolated from type I and type IIb skeletal muscle. *Am. J. Physiol.*, **270**, C673–C678.
62. Russell, A.J., Hartman, J.J., Hinken, A.C., Muci, A.R., Kawas, R., Driscoll, L., Godinez, G., Lee, K.H., Marquez, D., Browne, W.F. *et al.* (2012) Activation of fast skeletal muscle troponin as a potential therapeutic approach for treating neuromuscular diseases. *Nat. Med.*, **18**, 452–455.
63. de Winter, J.M., Buck, D., Hidalgo, C., Jasper, J.R., Malik, F.I., Clarke, N.F., Stienen, G.J., Lawlor, M.W., Beggs, A.H., Ottenheijm, C.A. *et al.* (2013) Troponin activator augments muscle force in nemaline myopathy patients with nebulin mutations. *J. Med. Genet.*, **50**, 383–392.
64. Lee, E.J., De Winter, J.M., Buck, D., Jasper, J.R., Malik, F.I., Labeit, S., Ottenheijm, C.A. and Granzier, H. (2013) Fast skeletal muscle troponin activation increases force of mouse fast skeletal muscle and ameliorates weakness due to nebulin-deficiency. *PLoS One*, **8**, e55861.
65. Hooijman, P.E., Beishuizen, A., de Waard, M.C., de Man, F.S., Vermeijden, J.W., Steenvoorde, P., Bouwman, R.A., Lommen, W., van Hees, H.W., Heunks, L.M. *et al.* (2014) Diaphragm fiber strength is reduced in critically ill patients and restored by a troponin activator. *Am. J. Respir. Crit. Care Med.*, **189**, 863–865.
66. de Winter, J.M., Joureau, B., Sequeira, V., Clarke, N.F., van der Velden, J., Stienen, G.J., Granzier, H., Beggs, A.H. and Ottenheijm, C. A. (2015) Effect of levosimendan on the contractility of muscle fibers from nemaline myopathy patients with mutations in the nebulin gene. *Skelet. Muscle*, **5**, 12.
67. Chan, Y., Tong, H.Q., Beggs, A.H. and Kunkel, L.M. (1998) Human skeletal muscle-specific alpha-actinin-2 and -3 isoforms form homodimers and heterodimers in vitro and in vivo. *Biochem. Biophys. Res. Commun.*, **248**, 134–139.
68. Lo, H.P., Cooper, S.T., Evesson, F.J., Seto, J.T., Chiotis, M., Tay, V., Compton, A.G., Cairns, A.G., Corbett, A., MacArthur, D.G. *et al.* (2008) Limb-girdle muscular dystrophy: diagnostic evaluation, frequency and clues to pathogenesis. *Neuromuscul. Disord.*, **18**, 34–44.
69. Brooke, M.H. and Kaiser, K.K. (1970) Muscle fiber types: how many and what kind? *Arch. Neurol.*, **23**, 369–379.
70. Cooper, S.T., Lo, H.P. and North, K.N. (2003) Single section Western blot: improving the molecular diagnosis of the muscular dystrophies. *Neurology*, **61**, 93–97.
71. Ilkovski, B., Nowak, K.J., Domazetovska, A., Maxwell, A.L., Clement, S., Davies, K.E., Laing, N.G., North, K.N. and Cooper, S.T. (2004) Evidence for a dominant-negative effect in ACTA1 nemaline myopathy caused by abnormal folding, aggregation and altered polymerization of mutant actin isoforms. *Hum. Mol. Genet.*, **13**, 1727–1743.
72. Marttila, M., Lemola, E., Wallefeld, W., Memo, M., Donner, K., Laing, N.G., Marston, S., Gronholm, M. and Wallgren-Pettersson, C. (2012) Abnormal actin binding of aberrant beta-tropomyosins is a molecular cause of muscle weakness in TPM2-related nemaline and cap myopathy. *Biochem. J.*, **442**, 231–239.
73. Bing, W., Fraser, I.D. and Marston, S.B. (1997) Troponin I and troponin T interact with troponin C to produce different Ca2 +-dependent effects on actin-tropomyosin filament motility. *Biochem. J.*, **327**, 335–340.
74. Ottenheijm, C.A., Witt, C.C., Stienen, G.J., Labeit, S., Beggs, A. H. and Granzier, H. (2009) Thin filament length dysregulation contributes to muscle weakness in nemaline myopathy patients with nebulin deficiency. *Hum. Mol. Genet.*, **18**, 2359–2369.
75. Manders, E., Bogaard, H.J., Handoko, M.L., van de Veerdonk, M.C., Keogh, A., Westerhof, N., Stienen, G.J., Dos Remedios, C.G., Humbert, M., Dorfmuller, P. *et al.* (2014) Contractile dysfunction of left ventricular cardiomyocytes in patients with pulmonary arterial hypertension. *J. Am. Coll. Cardiol.*, **64**, 28–37.